EUROPEAN MECHANICAL SCIENCE

Research Article

e-ISSN: 2587-1110

Nanoindentation evaluation of mechanical and wear properties of Zn-3% Cu-9% Al alloy processed via ECAP

Serkan Ateş[1*]

[1]Mechanical Engineering Department, Faculty of Engineering and Architecture, Burdur Mehmet Akif Ersoy University, Burdur, 15030, Türkiye

Abstract: This study utilizes equal channel angular pressing (ECAP), also known as equal channel angular extrusion (ECAE), to induce severe plastic deformation in Zn-3% Cu-9%Al (ZCA-9 Al) alloy, resulting in ultrafine-grained structures. ECAP is an unconventional technique used to impart severe plastic deformation to materials, producing ultrafine-grained (UFG) structures. To obtain UFG structures, two well-known Routes, A and Bc, as well as a newly proposed Route, D, were employed and evaluated. Following ECAP processing, the samples were subjected to various tests to assess their tensile properties, creep resistance, and wear track deformation behavior. The results demonstrated that all tested Routes significantly enhanced the tensile properties and creep resistance of ZCA-9 Al alloys. Routes A, Bc, and D increased the ultimate tensile strength (UTS) by 14.42%, 16.34%, and 12.82%, respectively, although they had minimal impact on wear track deformation. Overall, the findings indicate that Routes A, Bc, and D can improve the tensile and creep properties of ZCA-9 Al alloy, with Route Bc showing slightly superior results, though it required a higher extrusion force.

Keywords: ECAP, Nanoindentation, Ultrafine Grained Structures, Tensile Strength, Creep, Wear.

1. Introduction

ECAP, or ECAE is a method proposed by V. M. Segal that have garnered attention in recent years for producing UFG materials. UFG materials undergo severe plastic deformation (SPD), which results in superior mechanical and physical properties compared to their original state. These materials typically have grain sizes ranging between 1 µm and 2 µm in diameter. Additionally, UFG materials exhibit high electrical resistivity and diffusivity, making them suitable for a wide variety of applications [1].

There are numerous techniques for producing UFG materials, including plasma processing, chemical and physical vapor deposition, inert gas condensation, and milling. However, these methods are not suitable for mass production. To achieve significant changes in material properties, high-angle grain boundaries (HAGB) are necessary, as they possess misorientation angles greater than 15 degrees [2].

For this reason, it is imperative to investigate non-traditional SPD techniques, such as ECAP, to address the shortcomings of conventional methods and to produce UFG materials with enhanced mechanical properties. UFG materials synthesized through SPD processes are typically characterized by granular HAGB. Grain boundaries play a pivotal role in grain size refinement by impeding dislocation motion within the material, which consequently improves both strength and hardness. The Hall-Petch relationship provides a robust explanation for the correlation between grain size, hardness, and strength. According to this principle, reducing the grain size brings the material closer to its theoretical strength limits, with maximum strength observed at approximately 20–30 nm [2-3].

If the UFG structure is preserved at elevated temperatures, where diffusion rates increase significantly, the material shows great potential for enabling superplastic forming at higher strain rates. For this reason, our focus is on ECAP as an SPD method for producing larger samples of UFG materials with low porosity. One of the key advantages of ECAP is that it strains the sample without causing dimensional changes. This is a significant benefit compared to other SPD methods, such as Accumulated Roll Bonding (ARB), which can induce

*Corresponding author:
Email: sates@mehmetakif.edu.tr

Cite this article as:

Ates , S. (2025). Nanoindentation evaluation of mechanical and wear properties of Zn-3% Cu-9% Al alloy processed via ECAP. *European Mechanical Science*, *9*(1): 25-37. https://doi.org/10.26701/ems.1616622

History dates:

Received: 10.01.2025, *Revision Request*: 26.02.2025, *Last Revision Received*: 28.02.2025, *Accepted*: 06.03.2025

dimensional changes and sometimes result in edge cracking or fracturing. ▶**Figure 1** provides a schematic illustration of the ECAP process.

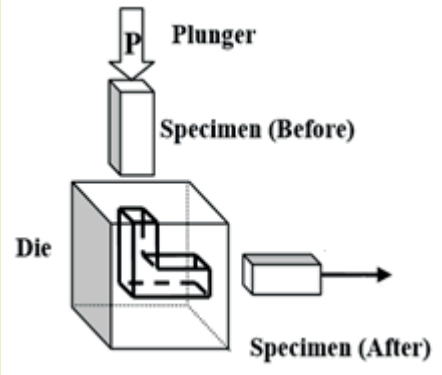

Figure 1. Schematic process of ECAP

Thus, ECAP is a widely used SPD method for achieving ultrafine-grained (UFG) structures by inducing large amounts of plastic deformation (with true strains greater than 10). A substantial body of evidence demonstrates that UFG structures processed through this method result in significant changes in the fundamental properties of the material [4–6]. ECAP also holds potential for large-scale production and commercial applications. Numerous studies have shown that the ECAP process improves the strength and ductility of materials in ways that may not be possible with conventional techniques.

For instance, Abioye et al. [7] found that subjecting AL 6063 alloys to ECAP enhanced their tensile properties. Similarly, Ding et al. [8] investigated three different processing Routes for Mg alloy and found that only Route A was effective in increasing strength. Jiang et al. [9] investigated how ECAP affects the room-temperature mechanical properties of cast Mg–9Al–Zn alloy, highlighting notable enhancements in yield strength, ultimate tensile strength, and elongation achieved through ECAE.

Martynenko et al. [10] studied the texture, microstructure, and mechanical behavior of magnesium alloy WE43 subjected to ECAP, concluding that the process improved both strength and ductility. Tolaminejad et al. [11] studied commercial purity aluminum subjected to ECAP using Route Bc. They found that the microstructure transitioned from elongated subgrains to ultrafine grains between passes 1 and 4, but no significant changes occurred between passes 4 and 8. They concluded that the first ECAP pass enhanced the mechanical properties by more than four times compared to the annealed condition.

Yang et al. [12] conducted a systematic analysis of the changes in microstructure, texture, and mechanical properties of extruded Mg-xY (x = 1, 5 wt.%) alloys during ECAP, utilizing optical microscopy, electron backscatter diffraction (EBSD), and uniaxial tensile testing. Their findings revealed that the Mg-5Y alloy experienced notable improvements in strength and elongation post-ECAP, with yield strength, ultimate strength, and elongation increasing by 10%, 6%, and 72%, respectively.

A notable advantage of ECAP lies in its ability to deform materials without altering the sample's cross-sectional area. Furthermore, the same material can undergo repeated processing by varying its orientation, referred to as different Routes. With an increasing number of passes, the material experiences progressively higher levels of deformation. These varying orientations result in the development of distinct substructures. Among the available ECAP Routes, A and Bc have demonstrated exceptional efficacy in enhancing mechanical properties and exerting a profound influence on the microstructure. The shear plane and the sample's rotation after successive passes for Routes A and Bc are illustrated in ▶**Figure 2**(a), ▶**Figure 2**(b) and ▶**Figure 2**(c), respectively.

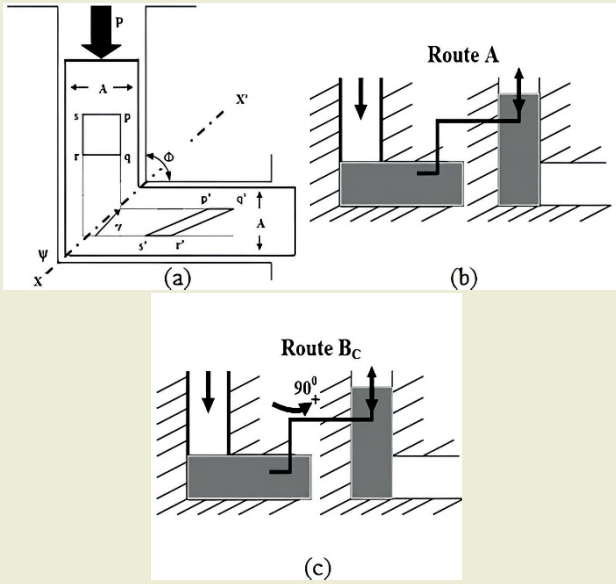

Figure 2. Different ECAP processing Routes. [13-14]

Route A produces elongated grains with a lamellar structure, formed by a gradual increase in the misorientation angle between adjacent grains. Conversely, Route Bc facilitates the development of a uniform microstructure comprising equiaxed grains, which are more rapidly delineated by high-angle grain boundaries (HAGB). Equiaxed grains are characterized by their nearly identical dimensions in all directions, providing a greater number of slip planes. This structural attribute significantly contributes to enhanced strength and ductility. In addition to Routes A and Bc, this study examines a new Route, named Route D, as shown in ▶**Figure 3**.

In Route D, the sample is rotated along the X-axis after each consecutive pass, a strategy designed to more

efficiently produce a uniform microstructure with equiaxed grains separated by high-angle grain boundaries (HAGB). In addition to the chosen Routes, essential factors like die angle, extrusion temperature, and extrusion speed significantly influence the ECAP process. Thang et al. [15] determined that, among seven different Routes, a 90° die angle was the most effective for achieving significant grain size reduction. This finding reinforces the suitability of ECAP as a method for obtaining a refined equiaxed microstructure, with a range of Routes and extrusion angles available to customize the microstructure according to specific requirements.

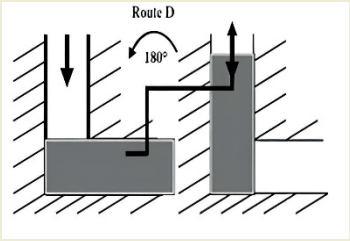

Figure 3. Route D

This study focused on Zn-Al alloys due to their widespread engineering applications. Savaskan et al. [16] noted that Zn alloys with 2–3% Cu offer high tensile strength, creep resistance, and wear resistance but become dimensionally unstable above 100°C. Zn-Al alloys are valued for their affordability, machinability, corrosion resistance, and superior surface finish compared to cast iron, with mechanical properties similar to low-carbon steel and aluminum. Their high damping capacity makes them suitable for noise and vibration reduction, though enhancing damping often compromises strength, posing a challenge in balancing both properties.

Zn-Al alloys with superior mechanical properties can be achieved through the addition of copper (Cu) or titanium (Ti), even without employing alternative forming techniques; however, this approach results in a reduction in ductility. Furthermore, the material's microstructure plays a pivotal role in determining its mechanical characteristics. ECAP, as an innovative and non-conventional processing method, holds significant potential for refining microstructures and generating ultrafine-grained (UFG) materials. Therefore, studying the impact of ECAP on the tribological and mechanical behaviors of Zn-Al alloys is crucial.

In this study, the tensile, creep, nanoindentation, scratch, and wear properties of cast and ECAP-processed Zn-9%Al-3%Cu alloys under various conditions were evaluated using nanoindentation instead of conventional testing methods. Additionally, the research analyzed the microstructural evolution of these alloys during ECAP, employing processing Routes A, Bc, and the newly proposed Route D.

2. Material and Methods

The ECAP process used a servo-hydraulic MTS machine with a 315 kN press to extrude samples through a die with two identical square channels, aided by a plunger. The system included a main block, center block, and supporting block, securely fastened with bolts.

Figure 4 shows the ECAP setup and a schematic of the die, featuring two channels intersecting at a 90° angle (Φ) with an outer arc angle (ψ) of 0°. Temperature was monitored using thermocouples placed 2 mm from the channel and within the environmental chamber enclosing the setup.

The extrusions were conducted at 650°C (±5°C), the minimum temperature to prevent shear cracks and control grain growth. Samples, made from as-cast ZCA-9 alloy (Zn-9%Al-3%Cu with trace Ti and Cr), were machined to dimensions of 6.35 × 6.35 × 35.75 mm.

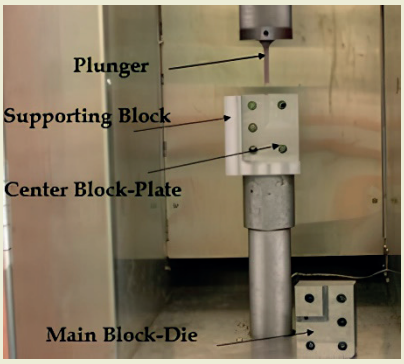

Figure 4. Photograph illustrating the ECAP setup

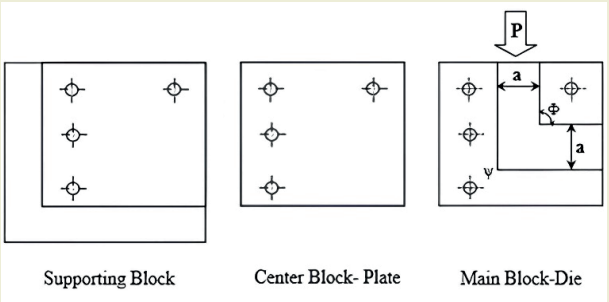

Figure 5. Schematic representation of the supporting block, center block, and main block of the ECAP die.

The sample was coated with molybdenum disulfide (MoS_2) paste, placed in the die's vertical channel, and heated for 15 minutes to reach the processing temperature before being extruded at a constant rate of 10 mm/min.

Following the initial extrusion, samples underwent processing via Routes A, BC, and D, with up to eight passes through the 90° die. The applied load was continuously monitored and recorded using a load cell.

2.1. Mechanical Testing

Tension Testing

A uniaxial tensile test was conducted at room temperature using an MTS machine with a 44 kN load cell on samples processed via Routes A, BC, and D. Tests followed ASTM E8 standards, with a strain rate of 1.74×10^{-3} s^{-1}. Three samples per Route were tested, averaged, and prepared to dimensions of 30 × 3 × 2.1 mm.

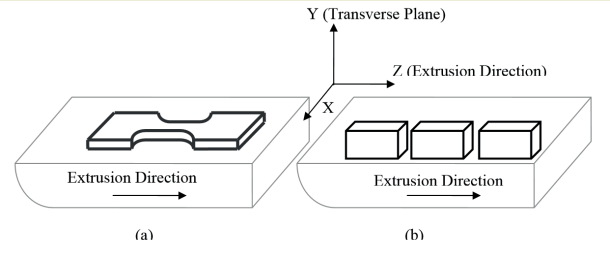

Figure 6. Schematic representation of the cutting orientation for (a) tensile and (b) compression samples, aligned parallel to the extrusion direction.

The samples were prepared in a dog bone shape with a rectangular cross-section, aligned parallel to the extrusion direction, and polished with 0.05 µm colloidal silica to eliminate surface imperfections. The gauge section was finalized at 10 × 3 × 2 mm. Strain gauges and a deflectometer were used to record strain and displacement during testing, with load-displacement data captured by a data acquisition system to calculate engineering stress (σ) and strain (ε):

$$\text{Engineering Stress, } \sigma = \frac{P}{A_0} \quad (1)$$

$$\text{Engineering Strain, } \varepsilon = \frac{(L-L_0)}{L} \quad (2)$$

Elongation was determined as:

$$\text{Elongation } (\%), \quad \% = \frac{L-L_0}{L_0} x100 \quad (3)$$

where L_0 is the gauge length before pulling depending on the size of the sample tested.

Nano hardness test

Nano hardness testing, also known as nanoindentation, involves measuring the depth of indentations on a nanometer scale. Nanoindentation tests using the MTS Nanoindenter XP were performed to assess the hardness and Young's modulus of the ZCA-9 alloy in its as-cast state and after ECAP processing. A Berkovich indenter created indentations at a depth of 1000–1500 nm with a strain rate of 0.05 s^{-1}. The schematic view of the ECAP-processed specimen is shown in ▶Figure 7.

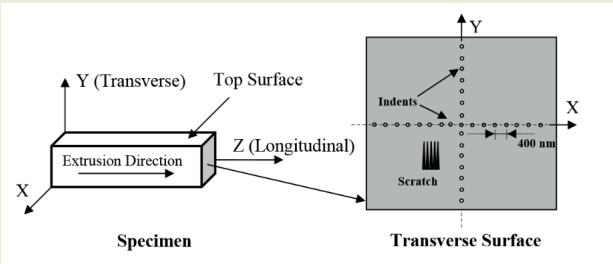

Figure 7. Schematic view of nanoindentation test on the transverse surface of the as-cast and ECAP processed alloy.

A series of fifteen nanoindents was conducted sequentially along the X and Y axes, with a spacing of 400 nm between each indent, to ensure that hardness remained consistent with depth along the axes. The indentation load and corresponding depths were recorded continuously during the tests, with a representative load-displacement curve shown in ▶Figure 8.

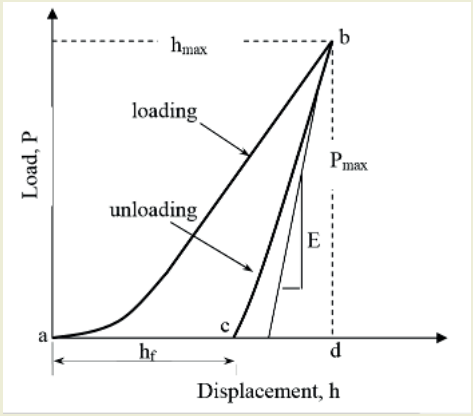

Figure 8. Schematic representation of a typical load-displacement curve generated during nanoindentation testing.

In nano hardness testing, the predetermined load is gradually and uniformly applied to the indenter, causing it to penetrate the sample (represented by curve AB in ▶Figure 8). At point B, the material's resistance matches the applied load, halting further penetration. As the load is gradually reduced, the indentation undergoes elastic recovery, producing the unloading curve BC. The material's Young's modulus (E) is determined from the slope of the linear portion of the unloading curve and is calculated as:

$$E = \frac{dP}{dh} \quad (4)$$

The hardness of the material (H) can be determined as:

$$H = \frac{P_{max}}{A} \quad (5)$$

where P_{max} represents the maximum indentation load (point B), and AAA denotes the projected area of the indentation impression.

Nano scratch Testing

Nano scratch tests using the MTS Nano Indenter XP evaluated the scratch properties of as-cast and ECAP-processed materials. Five 500 µm-long scratches were made on longitudinal and transverse surfaces using a Berkovich indenter. The applied load increased linearly from 0 to 90 mN at 10 µm/s. Parameters such as load-displacement, lateral deflection, table position, and time were monitored, and friction coefficients were calculated as the lateral force to normal load ratio.

Creep Testing

Uniaxial tensile creep tests at room temperature assessed the creep strength of as-cast and ECAP-processed ZCA-9 samples under a constant 61 kg load (30 MPa stress). Samples, fabricated per ASTM E139 standards (5 mm diameter, 10 mm gauge length), were CNC machined for minimal heat and high surface quality. All but the as-cast samples were tested until failure. Displacement data were recorded using an extensometer and LVDT, with nominal strain (ε) calculated as the change in length (Δl) relative to the original length (l).

$$\varepsilon = \frac{\Delta l}{l_0} \tag{6}$$

2.2. Microstructural Characterization

Optical Microscope and Scanning Electron Microscope

Metallurgical analysis of as-cast, ECAP-processed, and heat-treated ZCA-9 alloy was conducted using optical microscopy and Scanning Electron Microscope (SEM) for grain and particle size evaluation, while Environmental Scanning Electron Microscope (ESEM) analyzed alloy phases. Samples were sectioned transversely with a diamond blade, then ground with SiC paper (240–600 grit) and polished with alumina abrasives (5–0.05 µm).

OM and SEM Results

The microstructural changes in as-cast, as-ECAP, and post-ECAP alloys were analyzed using SEM. ▶**Figures 9(a) and 9(b)** display Backscattered Electrons Mode (BSEM) images at low magnification and secondary images at higher magnification of the as-cast ZCA-9 alloy.

The as-cast ZCA-9 alloy exhibits randomly distributed grains with a three-phase eutectic structure, where dark, grey, and white regions correspond to Al-rich, Zn-rich, and Cu-rich phases, respectively. A tree-stem-like eutectic structure containing η, α, and ε phases was determined, with EDS analysis presented in ▶**Figures 10–13**.

The η phase is dominant in Zn BSE images, the α phase in Al-scattered images, and the ε phase in Cu-scattered images. The as-cast ZCA-9 alloy also contains Al-rich dendrites and Zn-rich eutectic phases. Zhu et al. [17] reported similar dendritic structures in Zn-Al alloys, where reducing dendrite spacing enhances mechanical properties by minimizing microsegregation. Osorio et al. [18] and Turhal et al. [19] further confirmed that finer dendrite spacing improves tensile and yield strength while reducing porosity, particularly in Zn alloys with higher Al content.

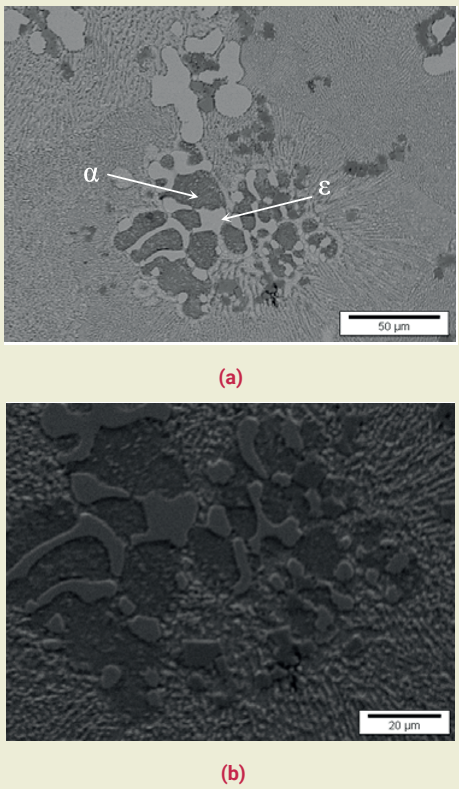

Figure 9. (a) Backscattered (b) Secondary images of as-cast ZCA-9 alloy.

ECAP-processed ZCA-9 alloys, contributing to improved mechanical properties, including increased strength and ductility. Optical micrographs (▶**Figures 14(a)–(d)**) show that a single ECAP pass refined the microstructure into a uniform equiaxed grain structure (average grain size: 0.24 µm). Grain boundary sliding (GBS), crucial for structural superplasticity, was facilitated by equiaxed grains and the spherical distribution of Al-rich phases, enhancing GBS efficiency compared to laminar structures.

In Route A, grain structures become fibrous and elongated along the extrusion direction due to the lack of rotation during successive ECAP passes, leading to a mixture of course and fine grains with limited homogeneity. Deformation zones around hard particles and reduced deformation band spacing accelerate the formation of UFG structures [22]. As a directional strain process, Route A causes strain to accumulate consistently, subdividing grains into cell blocks with varying slip systems [23]. This process promotes grain rotation toward stable orientations, forming high-angle grain boundaries (HAGB).

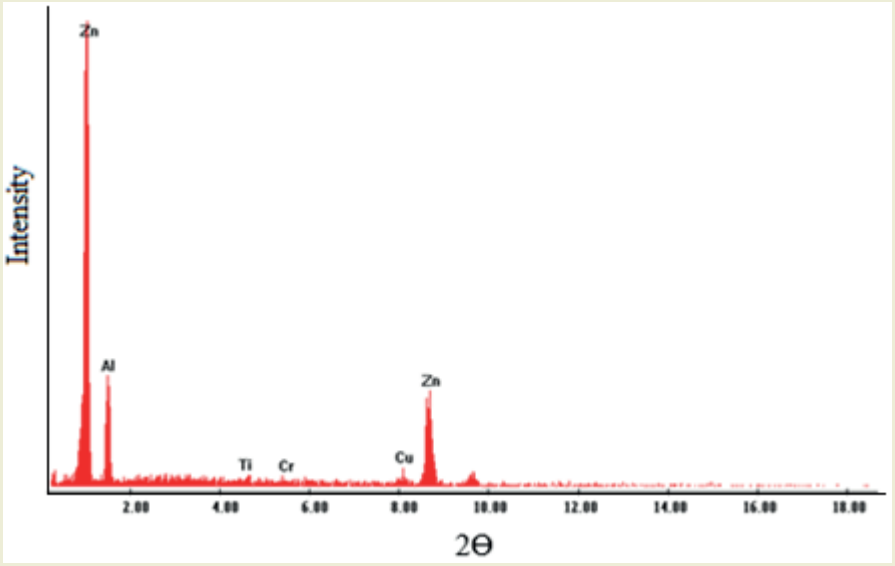

Figure 10. EDS spectrum of as-cast ZCA-9 alloy.

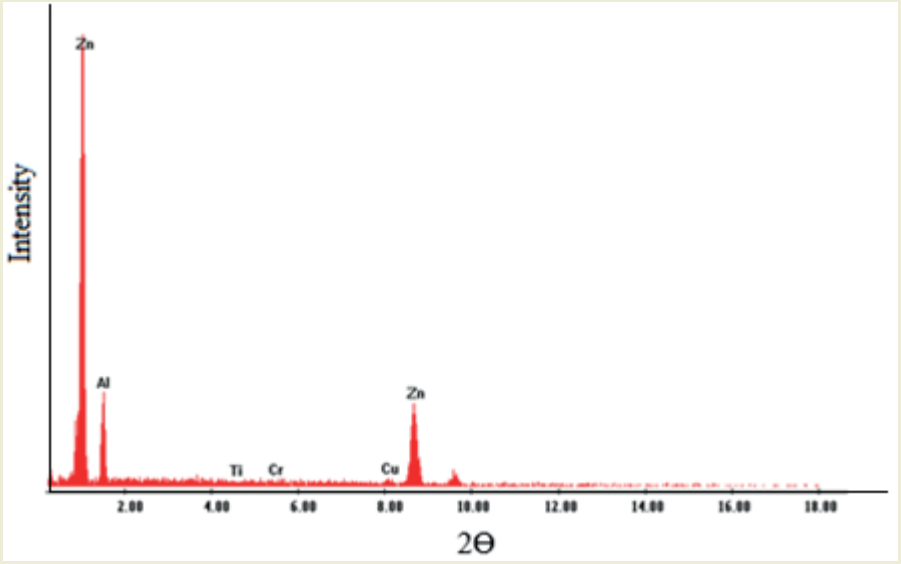

Figure 11. EDS spectrum of light phase of as-cast ZCA-9 alloy.

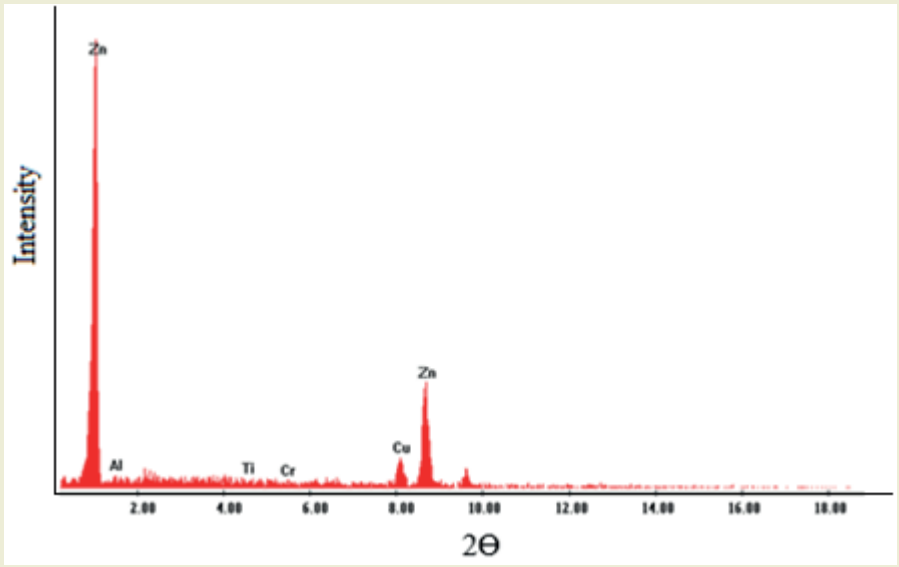

Figure 12. EDS spectrum of white phase of as-cast ZCA-9 alloy.

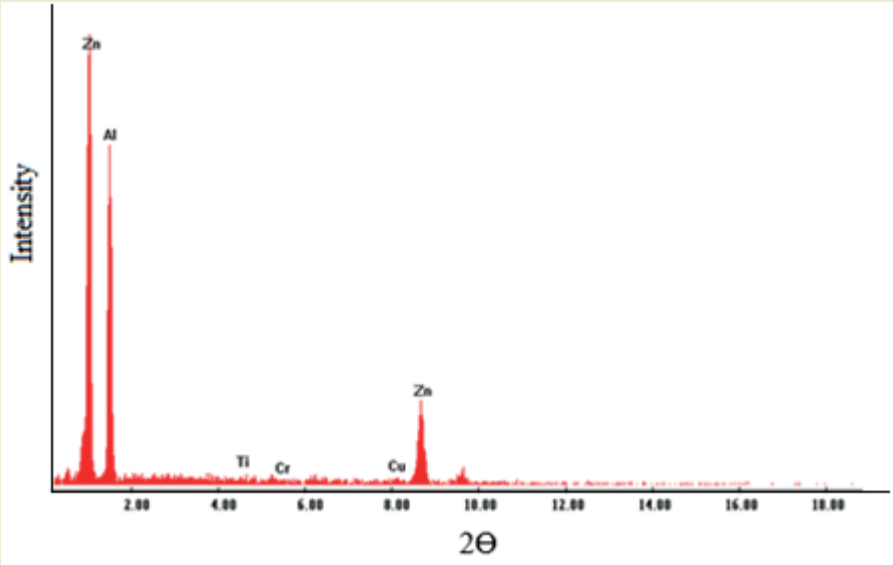

Figure 13. EDS spectrum of dark phase of as-cast ZCA-9 alloy.

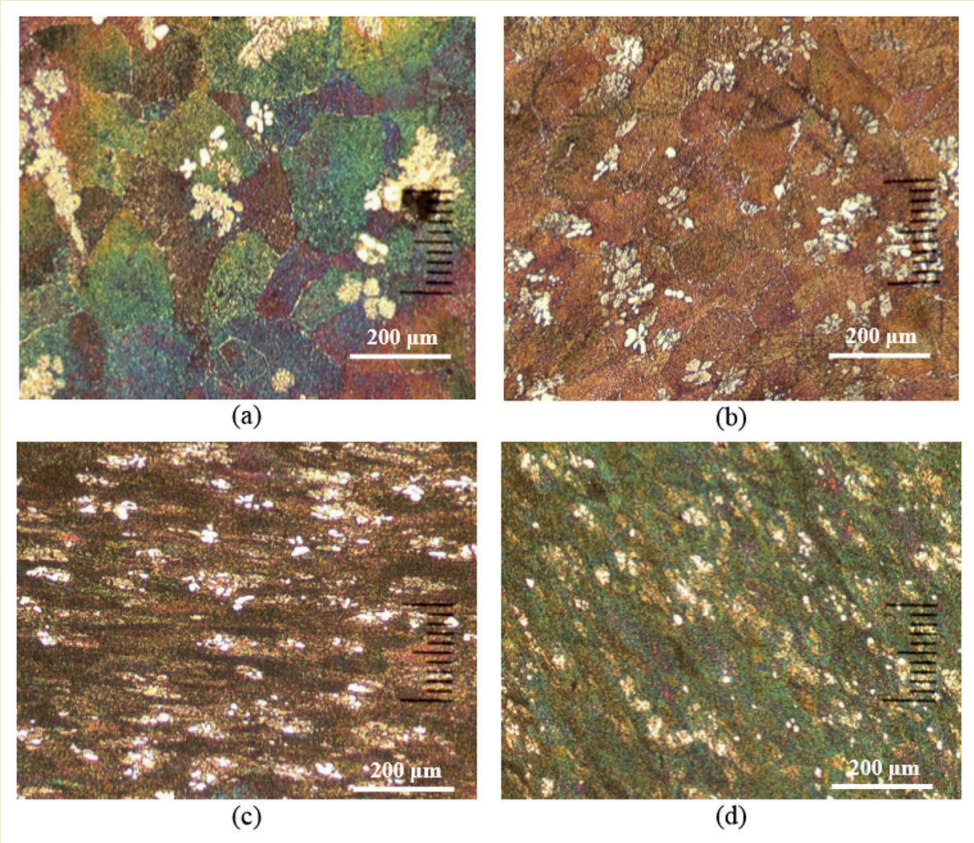

Figure 14. Optical micrographs illustrating typical microstructure of (a) as-cast, and ECAP processed sample up to (b) one pass, (c) Route A-two passes and (d) Route Bc-two passes.

3. Mechanical Results

3.1. ECAP Process

Figure 15(a) and (b) depict the variation in extrusion load as a function of displacement for the alloy during the ECAP process using Routes A and BC.

As shown in ▶**Figures 15(a) and (b)**, at the start of the ECAP process, the extrusion force rises sharply as the plunger advances, but it quickly stabilizes due to the material's yield resistance. Once the yield resistance is overcome and the peak load is reached, the extrusion load decreases, then increases again to a level close to or exceeding the previous peak before dropping as the process concludes. In ▶**Figure 15(a)**, the extrusion force remains constant for the first and second passes but

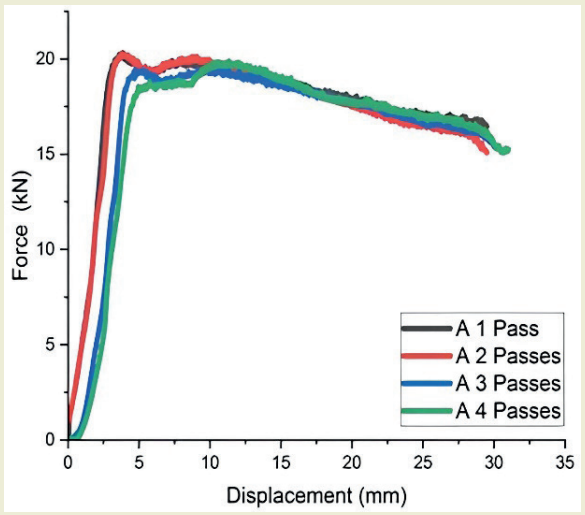

(a)

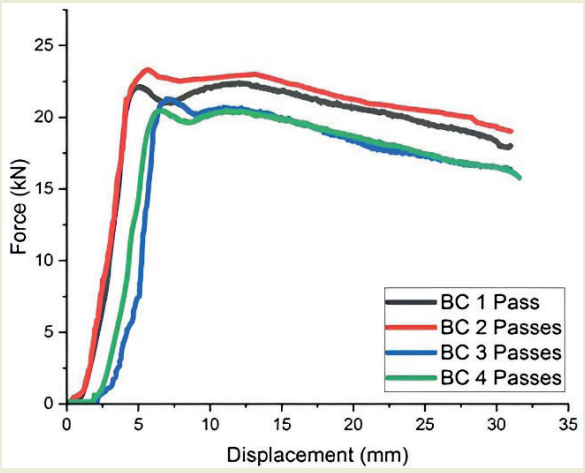

(b)

Figure 15. Force-displacement curves of the ZCA-9 samples from the ECAP process of different numbers of passes. (a) Route A, (b) Route Bc.

begins to decline thereafter. For Route Bc, the extrusion load increases from the first to the second pass and then follows a decreasing trend similar to Route A. Notably, the extrusion force required for the ECAP process is higher for Route Bc compared to Route A. This increased force requirement for Route Bc can be attributed to the presence of elongated grains and microbands aligned with the extrusion direction. Similar findings were reported by Purcek et al. [24] during high-temperature extrusion of Zn-27%Al alloy. It is also worth noting that the geometry of the die significantly influences the deformation process. The strain experienced by the material during ECAP is highly dependent on the channel angle (Φ) and the outer arc curvature angle (Ψ). The total strain intensity during the process can be determined using the following equation:

$$\varepsilon_P = \frac{N}{\sqrt{3}}\left[2\cot\left(\frac{\phi+\psi}{2}\right) + \cos\ ec\left(\frac{\phi+\psi}{2}\right)\right] \quad (7)$$

In the equation, N represents the number of passes, Ψ is the angle of the arc of curvature, and Φ is the angle between the channels (refer to ▶**Figure 2**). The equation indicates that the number of passes, N, is directly proportional to the efficiency of the ECAP process. According to Thang et al. [15], a channel angle Φ of 90° is the most effective for achieving significant grain size reduction. Nagasekhar et al. [25], through finite element analysis, studied the deformation behavior of extruded materials and determined that optimal strain homogeneity, minimal dead zone formation, and no adverse effects could be achieved with a Φ angle of 90° and a Ψ angle of 20°.

In this study, the die angles were set to Φ=90o and Ψ=20o to examine the effects of ECAP on the mechanical and tribological properties of the Zn-3%Cu-9%Al alloy. Determining the optimal die angles is crucial for obtaining ultrafine-grained (UFG) materials with fewer ECAP passes, thereby making the process more time- and cost-efficient. The results indicate that Route Bc is the most effective in producing equiaxed fine-grained materials. However, this Route requires higher extrusion forces compared to Route A. Unfortunately, data on extrusion forces for Route D is unavailable, preventing any conclusions regarding its performance.

Tension Test Results

The tensile tests aimed to evaluate the mechanical properties of ECAP-processed samples, focusing on UTS and yield strength (YS). Engineering stress-strain curves for samples processed through Routes A, Bc, and D are shown in ▶**Figures 16(a)–(c)**.

All three engineering stress-strain diagrams reveal a substantial increase in ultimate tensile strength (UTS) following the first ECAP pass. Route A achieved its maximum UTS after the first pass, Route Bc reached its peak after the second pass, and Route D attained its highest UTS after the third pass. After reaching a peak UTS value, additional passes led to a reduction in both UTS and YS. The peak UTS values were similar among the Routes, with the highest observed for Route Bc. The UTS values increased by 14.42% for Route A, 16.34% for Route BC, and 12.82% for Route D. Additionally, each Route exhibited strain-softening behavior and improved ductility after successive passes, which is arguably the most noteworthy aspect of the engineering stress-strain diagrams. A substantial increase in ductility occurred without a significant decrease in tensile strength. These results suggest that Routes A, BC, and D can be used to enhance the tensile properties of ZCA-9 alloys.

The comparison with extrusion force data indicates that the force required for ECAP is influenced by the improved ductility in Route Bc, likely due to better grain refinement and reduced dislocation density from SPD. This effect is absent in Route A, where the lack of rotation between passes leads to repeated shear in the same direction, promoting a uniform microstructure and greater work-hardening. Extrusion data for Route

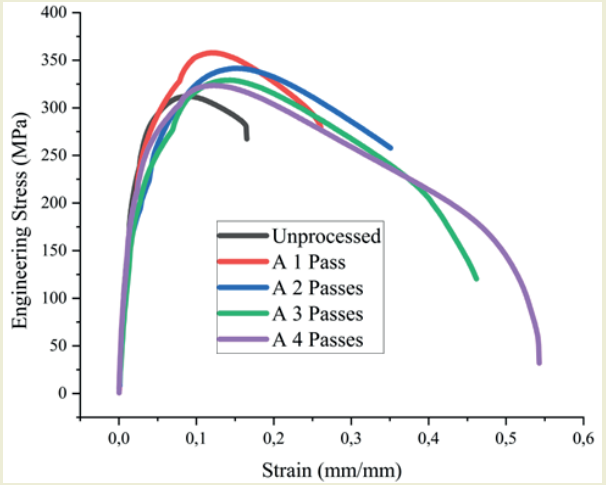

(a)

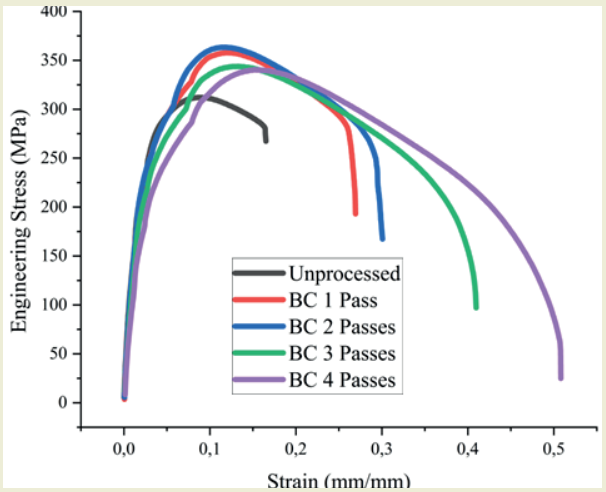

(b)

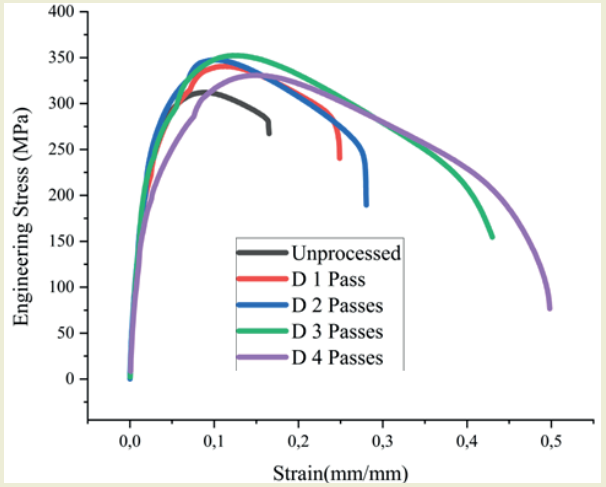

(c)

Figure 16. Engineering stress-strain curves for ZCA-9 samples processed through Route A (a), Route Bc (b), and Route D (c).

D are unavailable, preventing further analysis of its behavior.

Ramirez et al. [26] found that Route Bc significantly enhanced the tensile strength and ductility of Al-Si-Cu alloy by promoting a homogeneous and refined microstructure. Awasthi et al. [27] observed that Route BC enhanced tensile properties, including tensile strength and ductility, due to the development of refined grain structures. Similarly, Alateyah et al. [28] reported that Route A led to substantial grain refinement and the conversion of low-angle grain boundaries into high-angle grain boundaries, resulting in improved mechanical properties such as UTS and ductility. El-Shenawy et al. [38] found that ECAP processing using Route A for the AA2024 aluminum alloy significantly improved its tensile properties.

Creep Test Results

Figure 17 shows the displacement – time graph for the creep tests carried out on a single sample.

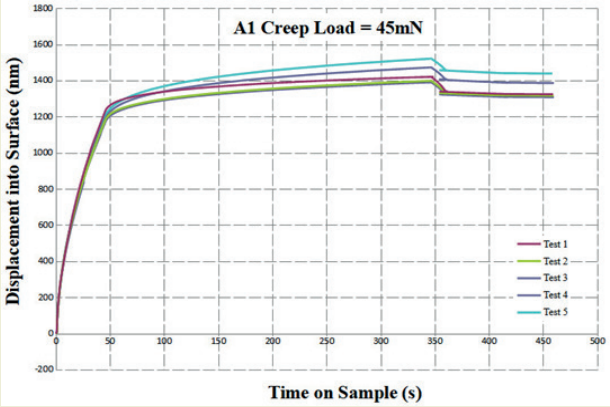

Figure 17. Displacement into surface – time graph for the 45 mN load test on Route A single pass sample.

Two phases typically observed in a creep test are clearly visible here. Displacement into the surface increases in the first region and continues to increase at a constant rate in the second region. After unloading, the displacement starts to decrease. Additionally, creep compliance graphs were obtained from the nanoindenter. Similar to the displacement versus time graph, creep compliance increases in the first and second phases. The creep compliance graph is shown in ▶**Figure 17**.

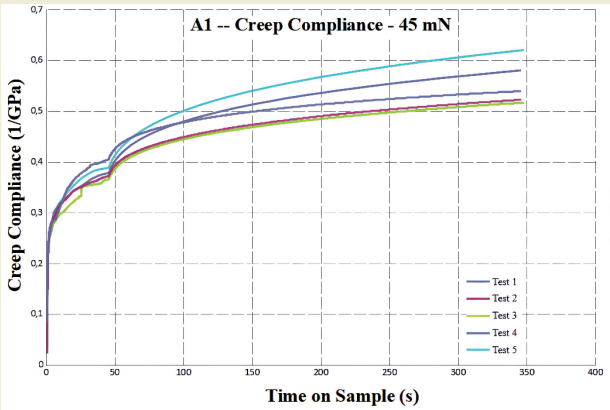

Figure 18. Creep compliance – time graph of Route A 1 pass sample.

https://doi.org/10.26701/ems.1616622

As shown in ▶**Figure 18**, variation in creep compliance is expected since the stress on the sample is constant and creep compliance is directly proportional to strain. The results for surface displacement and creep compliance were obtained from the nanoindenter for samples processed using Routes A, BC, and D. The stress exponent for the nanoindentation test was calculated by the software. ▶**Figure 19(a)–(c)** illustrates the average stress exponent as a function of the number of passes for Routes A, BC, and D, respectively.

The stress exponent is an important parameter for predicting creep behavior. For the sample processed by Route A, as shown in ▶**Figure 19 (a)**, significant changes in the stress exponent were observed at different passes. Even after the first pass, a notable reduction in the stress exponent value was observed. The same trend was seen across different loading conditions. Another significant drop in the stress exponent occurred after the third pass. After the fourth pass, the stress exponent increased for lower loads but continued to decrease for higher loads. A similar pattern was observed for Route Bc; however, for Route D, all stress exponent values increased. Route Bc showed similarities to Route A. Stress exponent values were almost identical for some loads but began to vary with the number of passes. Another notable drop in the stress exponent value was seen after the second pass, while the fourth pass caused almost no change. For Route D, changes in the stress exponent values were more linear compared to Routes A and Bc. After the fourth pass, the stress exponent values increased for all loads. The lowest stress exponent values were observed in the sample processed using Route Bc. Maier et al. [30] have related strain rate sensitivity (m) to the stress exponent as:

$$m = \frac{1}{n} \tag{8}$$

Strain rate sensitivity can indicate resistance to necking. The earlier decrease in stress exponent values may suggest increased strain rate sensitivity. El-Shenawy et al. [29] reported that ECAP processing of AA2024 aluminum alloy resulted in improved tensile properties and strain rate sensitivity. The uniform plastic strain distribution and refined microstructure due to ECAP led to a reduction in the stress exponent, enhancing the material's ability to accommodate strain rate variations. Similarly, Zhao et al. [31] found that ECAP processing, followed by annealing at various temperatures, significantly improved the strain rate sensitivity and mechanical properties of TA15 titanium alloy. The ECAP-induced grain refinement contributed to the observed drop in the stress exponent, indicating enhanced strain rate sensitivity. A similar observation can be made for the ZCA-9 alloy, as the stress exponent values are lower for the ECAP-processed samples. While the stress exponent is not the only parameter for evaluating a material's creep behavior, it provides valuable insights.

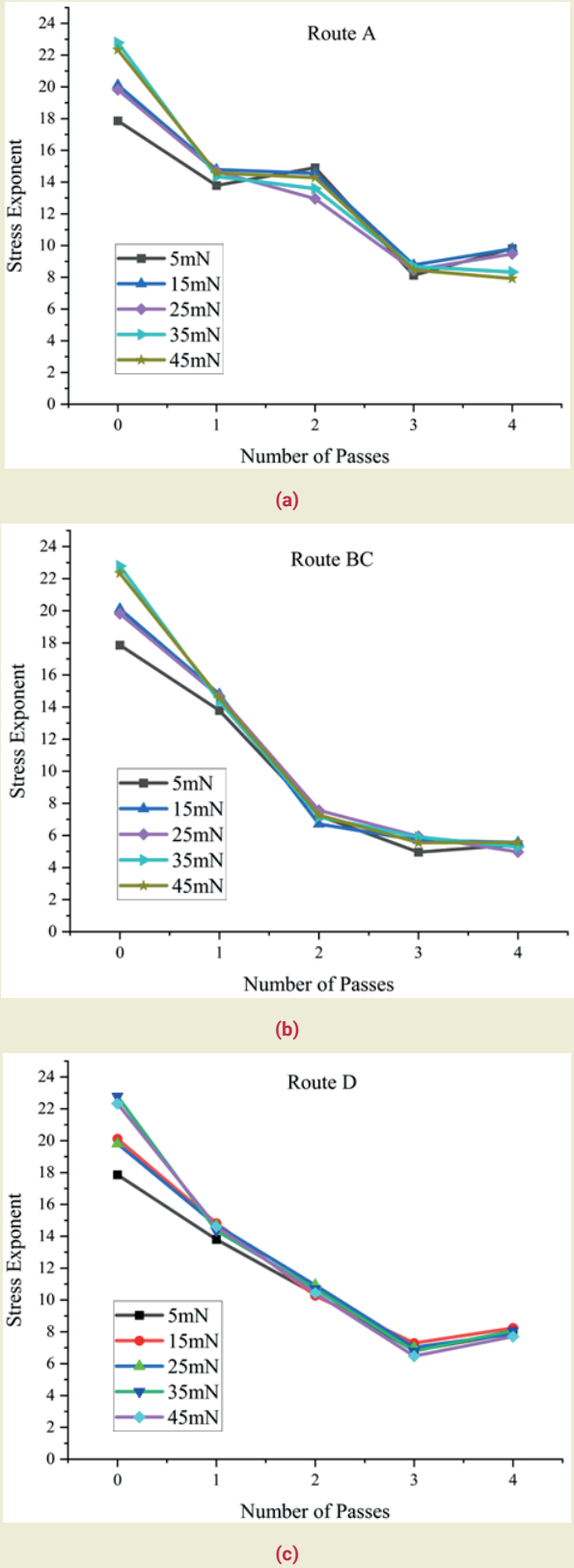

Figure 19. Stress exponent versus number of passes graphs for Route A (a), Route Bc (b) and Route D (c).

Wear Test Results

For the wear tests, a 500 μm wear path length was used, as previously mentioned. The values obtained are important for identifying the wear properties of the material. A higher wear track deformation value indicates lower wear resistance. ▶**Figure 20** shows the wear track deformation versus load on the sample and the number

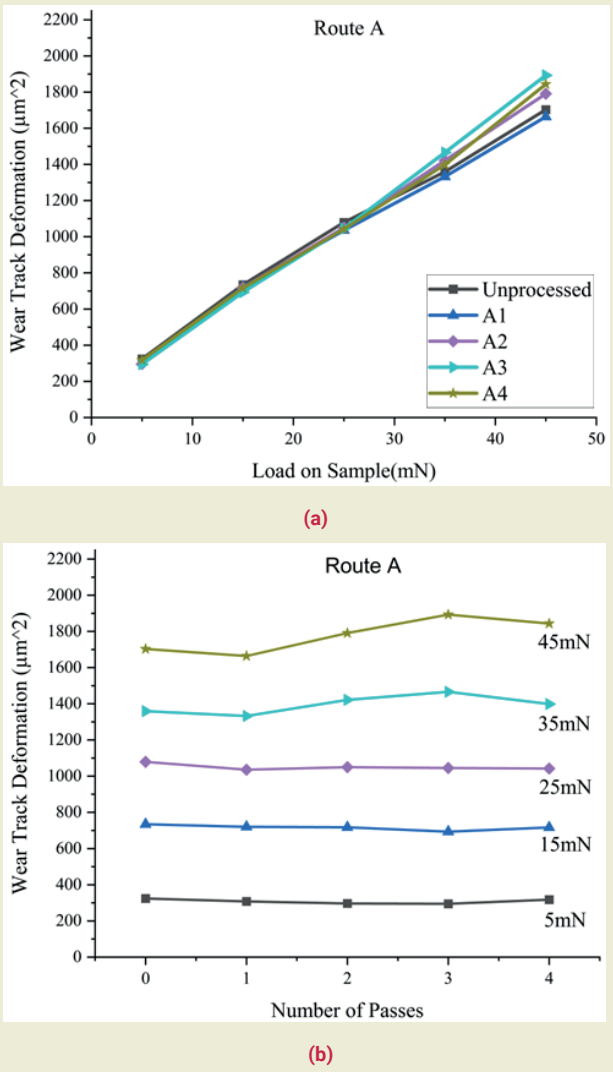

Figure 20. Wear track deformation versus load on sample and number of passing graphs for Route A.

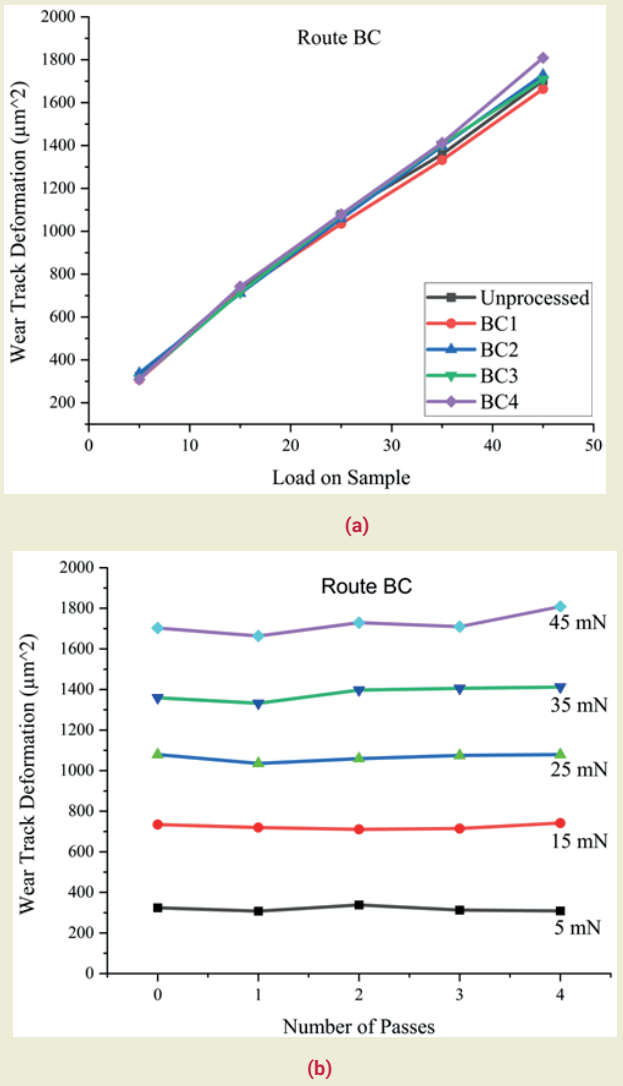

Figure 21. Wear track deformation versus load on sample and number of passing graphs for Route BC.

of passes for Route A.

As shown in ▶**Figure 21 (a)**, wear track deformation increases as the applied force increases. ▶**Figure 21 (b)** presents the wear track deformation versus the number of passes for Route A. As can be seen, the amount of material removed is almost linear, except for the 35 mN and 45 mN loads, where after the second pass, the amount of material removed increases. Yılmaz et al. [32] reported that wear track deformation was generally linear under various loads, except for specific intermediate loads like 35 mN and 45 mN, where an increase in wear was observed after subsequent ECAP passes. This was attributed to the complex interactions between the microstructure and applied loads during ECAP processing. ▶**Figure 21** shows the wear track deformation versus load on the sample and the number of passes for Route BC.

The wear track deformation for Route BC shows a similar linearity to that of Route A. However, unlike Route A, the wear track deformation for Route BC does not increase as much at the 35 and 45 mN loads. This suggests that samples processed by Route BC may be more suitable for such conditions, although the difference is not dramatic. Damavandi et al. [33] found that wear track deformation for samples processed by Route BC was more linear and exhibited less wear at higher loads compared to other Routes. This can be explained by the fact that Route BC produces a more uniform and homogeneous microstructure, which enhances wear resistance by providing a more uniform distribution of stress across the material. ▶**Figure 22** shows the wear track deformation versus load on the sample and the number of passes for Route D.

For Route D, the same linearity is observed. At the 35 mN load, wear track deformation starts to increase but remains more linear compared to Route A. However, at the 45 mN load, wear track deformation begins to resemble that of Route A. Therefore, it can be concluded that Route D falls somewhere between Routes A and Bc. Since the sample is rotated 180° after each pass, grain refinement is more homogeneous compared to Route A but less homogeneous than Route BC. Another reason could

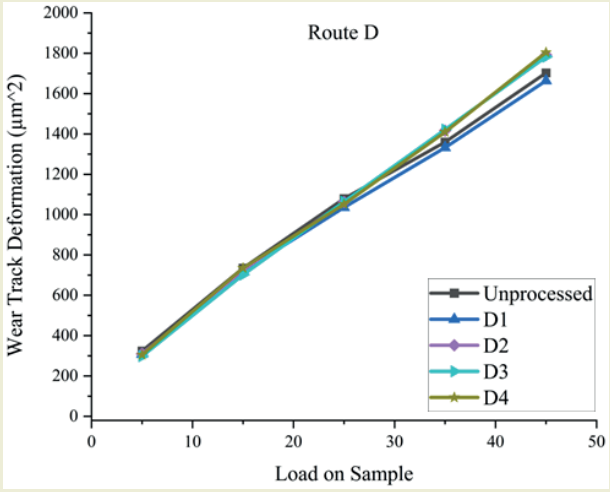

(a)

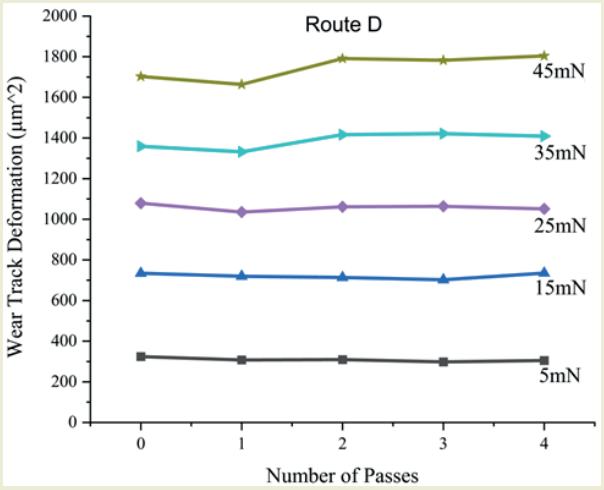

(b)

Figure 22. wear track deformation versus load on sample and number of passing graphs for Route D.

be that Route D generated more high-angle grain boundaries (HAGB) than Route A, which might have increased wear resistance by impeding dislocation movements.

4. Conclusion

The aim of this study was to investigate the tensile, creep, and wear properties of ECAP-processed ZCA-9 Al alloy and to test a newly proposed Route, referred to as Route D. The tension test results revealed that each Route can be used to improve the tensile strength of the ZCA-9 Al alloy. However, if optimal tensile strength is desired, Route BC is likely the best option. Additionally, the new Route, Route D, also shows promise for enhancing the tensile properties of the ZCA-9 Al alloy, but further studies are needed to fully understand its effects. For the creep tests, if only one or two passes are to be utilized, all tested Routes had significant effects on the stress exponent values. However, if higher creep resistance is desired, Route BC appears to be the best choice, as it exhibited the lowest stress exponent values for the third and fourth passes. Lastly, the wear test results indicate that ECAP processing did not have a significant effect on the wear resistance of the ZCA-9 Al alloy. If improved wear resistance is desired, other methods may need to be considered.

Research ethics

Not applicable.

Author contributions

The author solely conducted all stages of this research.

Competing interests

The author state no conflict of interest.

Research funding

None declared.

Data availability

The raw data can be obtained on request from the author.

Peer-review

Externally peer-reviewed.

Orcid

Serkan Ateş https://orcid.org/0000-0002-5858-5190

References

[1] Segal, V. M. (1999). Equal channel angular extrusion: From macromechanics to structure formation. Materials Science and Engineering: A, 271(1-2), 322–333.

[2] Whang, S. H. (Ed.). (2011). Nanostructured metals and alloys: Processing, microstructure, mechanical properties and applications. Elsevier.

[3] Naik, S. N., & Walley, S. M. (2020). The Hall–Petch and inverse Hall–Petch relations and the hardness of nanocrystalline metals. Journal of Materials Science, 55(7), 2661–2681.

[4] Valiev, R. Z., Krasilnikov, N. A., & Tsenev, N. K. (1991). Plastic deformation of alloys with submicron-grained structure. Materials Science and Engineering: A, 137, 35–40.

[5] Valiev, R. Z., Kozlov, E. V., Ivanov, Y. F., Lian, J., Nazarov, A. A., & Baudelet, B. (1994). Deformation behaviour of ultra-fine-grained copper. Acta Metallurgica et Materialia, 42(7), 2467–2475.

[6] Alexandrov, I. V., & Valiev, R. Z. (1999). Nanostructures from severe plastic deformation and mechanisms of large-strain work hardening. Nanostructured Materials, 12(5-8), 709–712.

[7] Abioye, O. P., Atanda, P. O., Osinkolu, G. A., Abioye, A. A., Olumor, I. D., Odunlami, O. A., & Afolalu, S. A. (2019). Influence of equal channel

angular extrusion on the tensile behavior of Aluminum 6063 alloy. Procedia Manufacturing, 35, 1337–1343.

[8] Ding, S. X., Lee, W. T., Chang, C. P., Chang, L. W., & Kao, P. W. (2008). Improvement of strength of magnesium alloy processed by equal channel angular extrusion. Scripta Materialia, 59(9), 1006–1009.

[9] Jiang, J., Wang, Y., Du, Z., Qu, J., Sun, Y., & Luo, S. (2010). Enhancing room temperature mechanical properties of Mg–9Al–Zn alloy by multi-pass equal channel angular extrusion. Journal of Materials Processing Technology, 210(5), 751–758.

[10] Martynenko, N. S., Lukyanova, E. A., Serebryany, V. N., Gorshenkov, M. V., Shchetinin, I. V., Raab, G. I., ... & Estrin, Y. (2018). Increasing strength and ductility of magnesium alloy WE43 by equal-channel angular pressing. Materials Science and Engineering: A, 712, 625–629.

[11] Tolaminejad, B., & Dehghani, K. (2012). Microstructural characterization and mechanical properties of nanostructured AA1070 aluminum after equal channel angular extrusion. Materials & Design, 34, 285–292.

[12] Yang, W., Quan, G. F., Ji, B., Wan, Y. F., Zhou, H., Zheng, J., & Yin, D. D. (2022). Effect of Y content and equal channel angular pressing on the microstructure, texture and mechanical property of extruded Mg-Y alloys. Journal of Magnesium and Alloys, 10(1), 195–208.

[13] Ferrasse, S., Hartwig, K. T., Goforth, R. E., & Segal, V. M. (1997). Microstructure and properties of copper and aluminum alloy 3003 heavily worked by equal channel angular extrusion. Metallurgical and Materials Transactions A, 28, 1047–1057.

[14] Langdon, T. G., Furukawa, M., Nemoto, M., & Horita, Z. (2000). Using equal-channel angular pressing for refining grain size. JOM, 52(4), 30–33.

[15] Tang, C. L., Hao, L. I., & Li, S. Y. (2016). Effect of processing route on grain refinement in pure copper processed by equal channel angular extrusion. Transactions of Nonferrous Metals Society of China, 26(7), 1736–1744.

[16] Savaskan, T., Pürçek, G., & Murphy, S. (2002). Sliding wear of cast zinc-based alloy bearings under static and dynamic loading conditions. Wear, 252(9-10), 693–703.

[17] Zhu, Y. H. (2001). Phase transformations of eutectoid Zn-Al alloys. Journal of Materials Science, 36(16), 3973–3980.

[18] Osório, W. R., & Garcia, A. (2002). Modeling dendritic structure and mechanical properties of Zn–Al alloys as a function of solidification conditions. Materials Science and Engineering: A, 325(1-2), 103–111.

[19] Turhal, M. Ş., & Savaşkan, T. (2003). Relationships between secondary dendrite arm spacing and mechanical properties of Zn-40Al-Cu alloys. Journal of Materials Science, 38, 2639–2646.

[20] Liu, Z., Li, P., Xiong, L., Liu, T., & He, L. (2017). High-temperature tensile deformation behavior and microstructure evolution of Ti55 titanium alloy. Materials Science and Engineering: A, 680, 259–269.

[21] Kumar, P., Xu, C., & Langdon, T. G. (2005). The significance of grain boundary sliding in the superplastic Zn–22% Al alloy after processing by ECAP. Materials Science and Engineering: A, 410, 447–450.

[22] Zhang, Y., Sao-Joao, S., Descartes, S., Kermouche, G., Montheillet, F., & Desrayaud, C. (2020). Microstructural evolution and mechanical properties of ultrafine-grained pure α-iron and Fe-0.02% C steel processed by high-pressure torsion: Influence of second-phase particles. Materials Science and Engineering: A, 795, 139915.

[23] Humphreys, F. J., & Hatherly, M. (2004). Recrystallization and related annealing phenomena (2nd ed.). Pergamon.

[24] Purcek, G., Altan, B. S., Miskioglu, I., & Patil, A. (2005). Mechanical properties of severely deformed ZA-27 alloy using equal channel angular extrusion. Materials Science and Technology, 21(9), 1044–1048.

[25] Nagasekhar, A. V., Tick-Hon, Y., Li, S., & Seow, H. P. (2006). Stress and strain histories in equal channel angular extrusion/pressing. Materials Science and Engineering: A, 423(1-2), 143–147.

[26] Ramirez, J. M. H., Bustamante, R. P., Merino, C. A. I., & Morquecho, A. M. A. (2020). Unconventional techniques for the production of light alloys and composites. Springer.

[27] Awasthi, A., Saxena, K. K., Dwivedi, R. K., Buddhi, D., & Mohammed, K. A. (2023). Design and analysis of ECAP processing for Al6061 alloy: A microstructure and mechanical property study. International Journal on Interactive Design and Manufacturing (IJIDeM), 17(5), 2309–2321.

[28] Alateyah, A. I., Alawad, M. O., Aljohani, T. A., & El-Garaihy, W. H. (2022). Effect of ECAP route type on the microstructural evolution, crystallographic texture, electrochemical behavior and mechanical properties of ZK30 biodegradable magnesium alloy. Materials, 15(17), 6088.

[29] El-Shenawy, M., Ahmed, M. M., Nassef, A., El-Hadek, M., Alzahrani, B., Zedan, Y., & El-Garaihy, W. H. (2021). Effect of ECAP on the plastic strain homogeneity, microstructural evolution, crystallographic texture and mechanical properties of AA2xxx aluminum alloy. Metals, 11(6), 938.

[30] Maier, V., Merle, B., Göken, M., & Durst, K. (2013). An improved long-term nanoindentation creep testing approach for studying the local deformation processes in nanocrystalline metals at room and elevated temperatures. Journal of Materials Research, 28(9), 1177–1188.

[31] Zhao, Y., Guo, H., Shi, Z., Yao, Z., & Zhang, Y. (2011). Microstructure evolution of TA15 titanium alloy subjected to equal channel angular pressing and subsequent annealing at various temperatures. Journal of Materials Processing Technology, 211(8), 1364–1371.

[32] Yilmaz, T. A., Totik, Y., Senoz, G. M. L., & Bostan, B. (2022). Microstructure evolution and wear properties of ECAP-treated Al-Zn-Mg alloy: Effect of Route, temperature and number of passes. Materials Today Communications, 33, 104628.

[33] Damavandi, E., Nourouzi, S., Rabiee, S. M., Jamaati, R., & Szpunar, J. A. (2021). Effect of Route BC-ECAP on microstructural evolution and mechanical properties of Al–Si–Cu alloy. Journal of Materials Science, 56, 3535–3550.